AlGaInAs/InP coupled-circular microlasers

Yongzhen Huang (黄永箴)*, Jiandong Lin (林建东), Qifeng Yao (姚齐峰), Xiaomeng Lü (吕晓萌), Yuede Yang (杨跃德), Jinlong Xiao (肖金龙), and Yun Du (杜 云)

State Key Laboratory on Integrated Optoelectronics, Institute of Semiconductors, Chinese Academy of Sciences, Beijing 100083, China

**Corresponding author: yzhuang@semi.ac.cn*

Received December 31, 2011; accepted March 28, 2012; posted online July 5, 2012

AlGaInAs/InP coupled-circular microlasers with radius of 10- and 2-μm width middle bus waveguide are fabricated by photolithography and inductively coupled plasma etching techniques. Room-temperature continuous-wave single-mode operation is realized with an output power of 0.17 mW and a side-mode suppression ratio of 23 dB at 45 mA. A longitudinal mode interval of 11 nm is obtained from the lasing spectra, and mode Q factor of 6.2×10^3 is estimated from 3-dB width of a minor peak near the threshold current. The mode characteristics are simulated by finite-difference time-domain technique for coupled-circular resonators. The results show that, in addition to the coupled modes, high-radial-order whispering gallery modes with travelling wave behaviors can also have high Q factors in the coupled-circular resonators with a middle bus waveguide.

OCIS codes: 140.3945, 140.5960, 230.5750.
doi: 10.3788/COL201210.091404.

Semicondcutor microlasers with whispering gallery modes (WGMs) have attracted great attention in the past two decades. Among these microlasers, microdisk laser with an ultrasmall cavity volume is the most common semiconductor microlaser[1]. However, directional emission is greatly limited in a circular-symmetry microdisk laser. Asymmetric circular resonators[2], spiral-shaped micropillars[3], elliptical microdisks[4], limaçon-shaped chaotic microcavities[5], and microdisk resonators evanescently coupled to a bus waveguide[6] have been investigated to realize directional emission microlasers. Recently, we realized continuous-wave (CW) electrically injected AlGaInAs/InP microcircular lasers at room temperature, which were connected to one or two output waveguides for directional emission[7,8].

Recently, mode radiation loss for microdisk resonators with pedestals was investigated by finite-difference time-domain (FDTD) technique[9]. For a circular microresonator connected to an output waveguide, the high-Q confined modes are usually the coupled modes between two WGMs with standing mode field patterns. However, high-Q confined modes with travelling mode field patterns are interesting for potential optical signal processing. Coupled-circular microresonators with a middle output waveguide can have high-Q coupled modes between WGMs, which can be predicted by FDTD technique[10]. Furthermore, optical bistable operation has been observed due to the transverse and degenerate mode competition in a coupled-circular GaInAsP/InP microlaser with a radius of 20 μm[11]. In this letter, we report the fabrication and characteristics of AlGaInAs/InP coupled-circular microlasers with a radius of 10 μm. Single-transverse-mode operation is observed with evident angular (longitudinal) mode structure in the lasing spectra, and mode Q factor of 6.2×10^3 is estimated from the full-width at half-maximum (FWHM) of a minor mode near the threshold current.

The coupled-circular microlasers were fabricated using a common edge-emitting AlGaInAs/InP laser wafer. The active region of the laser wafer comprised six compressively strained $Al_{0.24}GaIn_{0.71}As/Al_{0.44}GaIn_{0.49}As$ quantum wells sandwiched by 60-nm undoped graded AlGaInAs and 60-nm doped AlGaInAs cladding layers. The thicknesses of the quantum wells and barrier layers were 6 and 10 nm, respectively. The upper layers were p-InP and p^+-InGaAs contacting layers with the total thickness of 1 920 nm. The technique process used for fabricating the microlasers is similar to that in Ref. [11]. First, an 800-nm SiO_2 was deposited by plasma-enhanced chemical vapor deposition (PECVD) onto the laser wafer, after which the coupled-circular resonator patterns were transferred onto the SiO_2 layer using standard photolithography and inductively coupled plasma (ICP) etching techniques. Next, the laser wafer was etched approximately 5.5 μm using ICP technique with the patterned SiO_2 as masks. Figure 1(a) shows the scanning electron microscope (SEM) image of a coupled-circular microresonator, whereas Fig. 1(b) is the detail SEM image of the tangentially coupled region. After the ICP etching process, a chemically etching process was used to improve the smoothness of the etched side walls. The residual SiO_2 hard masks on the microcylinders were etched using diluted HF solution. A 450-nm SiO_2 insulating layer was deposited onto the wafer, and the SiO_2 layer on the top of circular resonators was etched using ICP etching process again for electrical injection. Finally, Ti-Pt-Au and Au-Ge-Ni were used as p-contact and n-contact metals, respectively.

After cleaving over the bus waveguide, the coupled circular microlasers were tested at room temperature

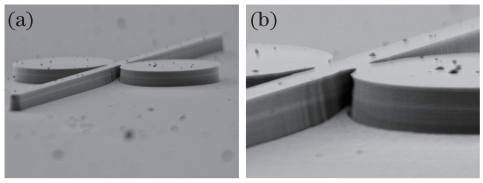

Fig. 1. SEM images of a coupled-circular resonator.

 © 2012 Chinese Optics Letters

without controlling temperature. The output power measured by an integrated sphere and applied voltage versus CW injection current for a coupled-circular microlaser with the circular radius of 10 μm and the bus waveguide width of 2 μm are plotted in Fig. 2. The output powers were 0.17 and 0.29 mW at the injection currents of 45 and 100 mA, respectively. Series resistor of 7 Ω was estimated by dividing the variation of the voltage to that of the injection current around the threshold current of 20 mA.

The laser spectra at CW injection currents of 25, 45, and 75 mA for the coupled-circular microlaser are plotted in Fig. 3. Two main modes with mode wavelengths of 1 549.9 and 1 561.0 nm, with an intensity difference of approximately 6 dB, can be observed in Fig. 3(a). The other minor modes were 20 dB less than the main mode at 1 561.0 nm. Single-mode operation with side-mode suppression ratios of 23 and 22 dB was reached at the injection currents of 45 and 75 mA, respectively, as shown in Fig. 3(b). The mode wavelength increased from 1 572.1 to 1 574.9 as the injection current increased from 25 to 75 mA, corresponding to the temperature rise of 28 K as the mode wavelength varied with the temperature at 0.1 nm/K. The lasing modes were at the wavelengths of 1 561.9 and 1 574.9 nm when the injection current was 45 and 75 mA, respectively. This phenomenon is caused by the increase of the peak wavelength of the gain spectrum with the temperature. Comparing with the optical bistability in the coupled-circular microlaser caused by the transverse and degenerate mode competition in Ref. [11], we have single-transverse-mode operation, as shown in the laser spectra in Fig. 3.

Assuming the wavelength intervals is the angular (longitudinal) mode interval and one period of the mode light path is the perimeter of the circular resonator, we can fit the longitudinal mode interval by $\delta\lambda = \lambda^2/2\pi R n_g$ and obtain the mode group indices of n_g = 3.52, 3.47, and 3.49 from the observed mode wavelength intervals. Single-mode operation indicates that the mode coupling is not influenced by the size mismatch of the circular resonators caused by imperfect fabrication process. In fact, coupled microcavities with a large mismatch of cavity size will result in lasing spectra with two set of modes.

Finally, mode characteristics were investigated by two-dimensional (2D) FDTD simulation for coupled-circular microlasers with a middle bus waveguide confined by

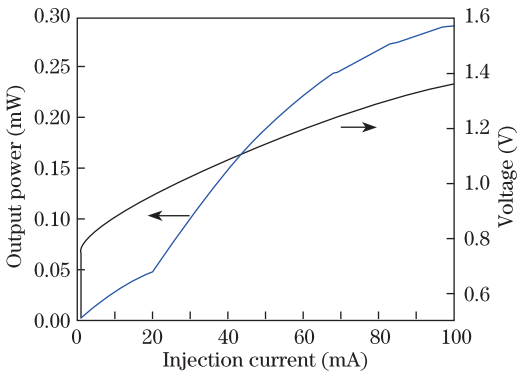

Fig. 2. Output power and applied voltage versus CW injection current at room temperature for a coupled-circular microlaser with a radius of 10 μm.

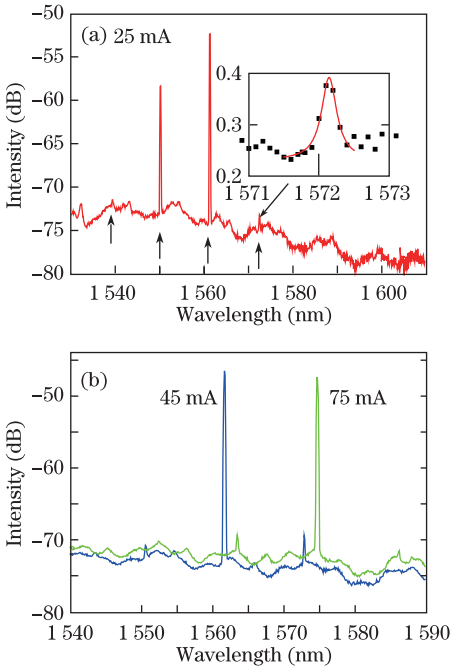

Fig. 3. Lasing spectra of the laser at the injecting currents of (a) 25, (b) 45, and 75 mA at room temperature. The inset shows the minor peak at 1 572.14 nm fitted by Lorentzian function.

insulator SiO_2 and p-electrode Ti and Au layers. In the simulation, the radius of coupled-circular and the width of the output waveguide were taken to be 3 and 0.4 μm, whereas the thicknesses of the SiO_2, p-electrode Ti, and Au layers were 0.45, 0.04, and 0.02 μm, respectively. The effective refractive index of the laser wafer was taken to be 3.2, and the refractive indices of the SiO_2, p-electrode Ti, and Au layers were 1.45, 3.7 + 4.5i, and 0.18 + 10.2i[12], respectively. Because the active region comprises compressively strained multiple quantum wells, we consider TE modes in the numerical simulation. Gaussian modulated cosine impulse was used as the exciting source $P(t) = \exp[-(t - t_0)^2/t_w^2]\cos(2\pi f_0 t)$ inside the resonator, where t_0 is the pulse center, t_w is the pulse half width, and f_0 is the center frequency of the pulse. A Courant time step of 0.0467 fs and a uniform mesh with the cell size of 20 nm were used in the simulation. In addition, t_0= 2.39 fs and t_w= 4.78 fs were taken for a wide-band exciting source centered at f_0 = 200 THz. The time-domain output of the z-direction magnetic field H_z was recorded at a selected monitor point inside the resonator as FDTD output. Then, Padé approximation was used to transform a late FDTD output from the time domain to the frequency domain[13]. The obtained intensity spectra for the coupled-circular microresonators laterally confined by SiO_2 and SiO_2/Ti/Au/air are plotted as the solid and the dashed lines in Fig. 4, respectively. The mode Q factors decreased as the confined layer was transformed from SiO_2 to SiO_2/Ti/Au/air.

Using a narrow-band exciting source with t_0=1.53 ps and t_w = 3.06 ps centered at a mode frequency, we simulate mode field patterns for the main peaks of the dashed line in Fig. 4 (i.e., for the resonator confined by SiO_2/Ti/Au/air). Under the narrow-band exciting sources, the mode Q factors of 3.0×10^3, 2.2×10^3,

8.6×10^3, 2.8×10^3, 1.2×10^4, 3.3×10^3, 4.0×10^3, and 1.1×10^4 were obtained for the modes at 197.96, 200.39, 203.24, 206.06, 208.50, 211.71, 212.18, and 213.75 THz, respectively. The obtained mode Q factors were approximately from 30% to 50% larger than those obtained from the multiple-mode intensity spectra in Fig. 4. We expect the mode Q factors obtained under narrow-band exciting sources to be more exact than those obtained under a wide-band exciting source. The obtained magnetic field patterns are plotted in Fig. 5 at the mode frequencies of 211.71, 212.18, and 213.75 THz. The field pattern in Fig. 5(a) is the third-order WGM $TE_{28,3}$ and symmetry relative to the bus waveguide, which is much stronger coupled to the bus waveguide than that in Figs. 5(b) and (c). The mode field patterns in Figs. 5(b) and (c) are coupled modes $TE_{28,3}$+$TE_{32,2}$, and $TE_{37,1}$+$TE_{32,2}$, which are antisymmetric relative to the bus waveguide. Based on simulated mode field patterns, we can also assign the peaks at 197.96, 200.39, 203.24, 206.06, and 208.50 THz of the solid line in Fig. 4 as $TE_{34,1}$+$TE_{29,2}$, $TE_{26,3}$, $TE_{35,1}$+$TE_{30,2}$, $TE_{27,3}$, and $TE_{36,1}$+$TE_{31,2}$. Here, $TE_{v,m}$ is WGM with v and m the angular and radial mode numbers, respectively, and $TE_{v1,m1}$+ $TE_{v2,m2}$ is a coupled mode between $TE_{v1,m1}$ and $TE_{v2,m2}$[14]. The coupled modes at 197.96, 203.24, and 208.50 THz are also coupled modes between the first- and the second-order WGMs with $v_1 - v_2 = 5$, having similar mode field patterns as Fig. 5(c). The higher-radial-order WGMs are less affected by the roughness of circular perimeter than the first-order WGM; therefore, realizing independent clockwise and counter-clockwise traveling wave operations from the higher radial order WGMs is easy because the low-radial-order WGMs have low Q factors in the coupled-circular resonator.

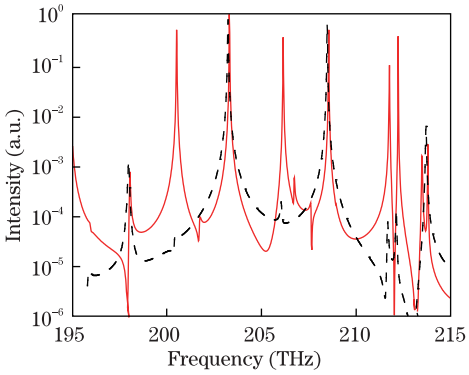

Fig. 4. Intensity spectra plotted as the solid and the dashed lines for the coupled-circular resonator laterally confined by SiO_2 layer and SiO_2/Ti/Au layer, respectively, with the radius of 3 μm and the width of the bus waveguide of 0.4 μm.

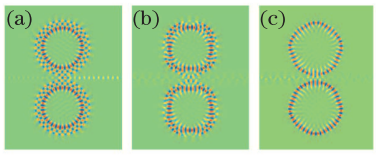

Fig. 5. Field patterns of the z-directional magnetic field component for the modes at the frequencies of (a) 211.71, (b) 212.18, and (c) 213.75 THz in the coupled-circular resonators with the middle bus waveguide.

In conclusion, we fabricate AlGaInAs/InP coupled-circular microlasers with a middle bus waveguide, and investigate output characteristics for a coupled-circular microlaser with radius of 10 μm. Clear angular-mode spectra are observed with the angular mode wavelength interval of approximately 11 nm and mode Q factor of 6.2×10^3 is obtained from the width of resonant peak. Furthermore, the numerical results show that the high-Q confined modes in the coupled-circular resonator are mainly the symmetric WGMs and antisymmetric coupled WGMs relative to the bus waveguide.

This work was supported by the National Natural Science Foundation of China under Grant Nos. 60777028, 60723002, 60838003, 61006042, and 61061160502.

References

1. S. L. McCall, A. F. J. Levi, R. E. Slusher, S. J. Pearton, and R. A. Logan, Appl. Phys. Lett. **60,** 289 (1992).
2. J. U. Nöckel, A. D. Stone, G. Chen, H. L. Grossman, and R. K. Chang, Opt. Lett. **21,** 1609 (1996).
3. G. D. Chern, H. E. Tureci, A. D. Stone, R. K. Chang, M. Kneissl, and N. M. Johnson, Appl. Phys. Lett. **83,** 1710 (2003).
4. S. K. Kim, S. H. Kim, G. H. Kim, H. G. Park, D. J. Shin, and Y. H. Lee, Appl. Phys. Lett. **84,** 861 (2004).
5. J. Wiersig and M. Hentschel, Phys. Rev. Lett. **100,** 033901 (2008).
6. J. V. Campenhout, P. Rojo-Romeo, P. Regreny, C. Seassal, D. V. Thourhout, S. Verstuyft, L. D. Cioccio, J. M. Fedeli, C. Lagahe, and R. Baets, Opt. Express. **15,** 6744 (2007).
7. S. J. Wang, J. D. Lin, Y. Z. Huang, Y. D. Yang, K. J. Che, J. L. Xiao, Y. Du, and Z. C. Fan, IEEE Photon. Technol. Lett. **22,** 1349 (2010).
8. J. D. Lin, Y. Z. Huang, Q. F. Yao, X. M. Lv, Y. D. Yang, J. L. Xiao, and Y. Du, Electron. Lett. **47,** 929 (2011).
9. Y. Yang, S. Wang, and Y. Huang, Chin. Opt. Lett. **8,** 502 (2010).
10. S. J. Wang, Y. D. Yang, and Y. Z. Huang, Opt. Lett. **35,** 1953 (2010).
11. J. Lin, Y. Huang, Y. Yang, Q. Yao, X. Lv, J. Xiao, and Y. Du, Opt. Lett. **36,** 3515 (2011).
12. M. A. Ordal, L. L. Long, R. J. Bell, S. E. Bell, R. R. Bell, R. W. Alexander, Jr., and C. A. Ward, Appl. Opt. **22,** 1099 (1983).
13. W. H. Guo, W. J. Li, and Y. Z. Huang, IEEE Microw. Wirel. Compon. Lett. **11,** 223 (2001).
14. Y. D. Yang, S. J. Wang, and Y. Z. Huang, Opt. Express **17,** 23010 (2009).